

Cortical parvalbumin neurons are responsible for homeostatic sleep rebound through CaMKII activation

Kazuhiro Kon^{1,6}, Koji L. Ode^{1,2}, Tomoyuki Mano^{1,2,3,7}, Hiroshi Fujishima², Daisuke Tone^{1,2}, Chika Shimizu², Shinnosuke Shiono¹, Saori Yada¹, Junko Yoshida Garçon², Mari Kaneko⁴, Yuta Shinohara^{2,8}, Riina R. Takahashi¹, Rikuhiro G. Yamada², Shoi Shi^{1,2,9}, Kenta Sumiyama^{5,10}, Hiroshi Kiyonari⁴, Etsuo A. Susaki^{1,2,11}, and Hiroki R. Ueda^{1,2,*}

1. Department of Systems Pharmacology, Graduate School of Medicine, The University of Tokyo, Bunkyo-ku, Tokyo 113-0033, Japan

10 2. Laboratory for Synthetic Biology, RIKEN Center for Biosystems Dynamics Research (BDR), Suita, Osaka 565-0871, Japan

3. Department of Information Physics and Computing, Graduate School of Information Science and Technology, The University of Tokyo, Bunkyo-ku, Tokyo 113-0033, Japan

4. Laboratory for Animal Resources and Genetic Engineering, RIKEN Center for Biosystems Dynamics Research, Chuou-ku, Kobe 650-0047, Japan

15 5. Laboratory for Mouse Genetic Engineering, RIKEN Center for Biosystems Dynamics Research (BDR), Suita, Osaka 565-0871, Japan

6. Present address: Kennedy Krieger Institute, Solomon H. Snyder Department of Neuroscience, Johns Hopkins University School of Medicine, Baltimore, MD 21205, USA

20 7. Present address: Computational Neuroethology Unit, Okinawa Institute of Science and Technology, Onna, Okinawa 904-0495, Japan

8. Present address: Division of Molecular Psychoimmunology, Institute for Genetic Medicine, Graduate School of Medicine, Hokkaido University, Sapporo 060-0815, Japan

9. Present address: International Institute for Integrative Sleep Medicine (IIIS), University of Tsukuba, Tsukuba, Ibaraki 305-8575, Japan

25 10. Present address: Laboratory of Animal Genetics and Breeding, Graduate School of Bioagricultural Sciences, Nagoya University, Chikusa-ku, Nagoya 464-8601, Japan

11. Present address: Department of Biochemistry and Systems Biomedicine, Juntendo University Graduate School of Medicine, Bunkyo-ku, Tokyo 113-8421, Japan

*. Correspondence (E-mail: uedah-tky@umin.ac.jp)

Abstract: The homeostatic regulation of sleep is characterized by rebound sleep after prolonged wakefulness, but the molecular and cellular mechanisms underlying this regulation are still unknown. We show here that CaMKII-dependent activity control of parvalbumin (PV)-expressing cortical neurons is involved in sleep homeostasis regulation. Prolonged wakefulness enhances cortical PV-neuron activity. Chemogenetic suppression or activation of cortical PV neurons inhibits or induces rebound sleep, implying that rebound sleep is dependent on increased activity of cortical PV neurons. Furthermore, we discovered that CaMKII kinase activity boosts the activity of cortical PV neurons, and that kinase activity is important for homeostatic sleep rebound. We propose that CaMKII-dependent PV-neuron activity represents negative feedback inhibition of cortical neural excitability, which serves as the distributive cortical circuits for sleep homeostatic regulation.

Main: The sleep-wake cycle is homeostatically regulated (1). The wakefulness history is recorded as “sleep need,” which is dissipated during the subsequent sleep. In addition to the brain-wide regulation (2), sleep homeostasis is locally regulated in the isocortex (3). In humans and rodents, delta power, a sleep need indicator, is locally enhanced in cortical regions that have been more activated during the preceding wakefulness (4, 5). Prolonged wakefulness results in “local sleep,” in which cortical neurons locally become silent like in sleep, despite the animal displaying an awake electroencephalogram (EEG) throughout the brain (6). These findings suggested that a local and minimal unit of the cortical circuit records their homeostatic sleep need and that the negative feedback system for sleep homeostasis can be found in general cortical circuits.

PV neurons, the most abundant GABAergic interneurons in the isocortex, contribute to feedforward and feedback inhibition in cortical microcircuits (7, 8). Thus, we hypothesized that activity control of cortical PV neuron is involved in the regulation of sleep homeostasis. Cortical PV neurons mature throughout postnatal development in terms of distribution, electrophysiological properties, and gene expression (9–13). Developmental dysfunctions in cortical PV neurons may responsible for the pathogenesis of autism spectrum disorder (ASD) (14, 15), and abnormal sleep symptoms are observed in many ASD patients and animal models of ASD (16). These findings suggest that the cortical PV-neuron maturation plays a role in physiological sleep-wake regulation. Indeed, sleep architecture and homeostasis are modulated in developmental-stage-dependent manner (17–19), and cortical PV-neuron activity is modulated by sleep-wake states (20, 21). Nonetheless, the role of cortical PV neurons in sleep homeostasis is unknown.

Sleep architecture and homeostasis are altered along with development.

We conducted long-term sleep phenotyping in developing mice after weaning (P21–84) to understand the developmental trajectory of sleep architecture (Fig. 1A). There was no significant change in daily sleep duration during the development (Fig. 1B). However, both P_{ws} and P_{sw} , the transition probabilities from wakefulness to sleep and sleep to wakefulness (22), increased continuously as the developmental stages progressed (Fig. 1, C to D). The light phase saw a greater increase in P_{ws} , while the dark phase saw a greater increase in P_{sw} (fig. S1, A to E). Consistent with this, sleep episodes in the dark phase became shorter than that in the light phase during the later developmental stages (fig. S1F).

We further performed a 6-hour sleep deprivation (SD) in individual mice aged 4, 8, and 12 weeks to validate sleep homeostasis in developing mice (fig. S2A). The rebound sleep was clearly observed at 8 and 12 weeks old, but less so at 4 weeks old (Fig. 1, E to G; fig. S2B). Wake

5

fragmentation (i.e., increased P_{ws}) and sleep consolidation (i.e., decreased P_{sw}) were induced in rebound sleep (**Fig. 1, H to I**). Similar to SD, rebound sleep responses were clearer at 8 and 12 weeks old than at 4 weeks old after MK-801 intraperitoneal (i.p.) administration (**Fig. 1, J to N; fig. S2C**). Long-term sleep phenotyping in developing mice revealed that the sleep-wake pattern and sleep homeostasis mature with post-weaning development.

Whole-brain distribution of PV neurons is altered along with development.

10

To understand the neural mechanisms underlying the developmental changes in sleep, we focused on PV neurons as a candidate neural basis for the changes. The mouse brains were collected at various stages of post-weaning development, followed by CUBIC-based tissue clearing for a whole-brain analysis of PV-neuron distribution (23, 24) (**Fig. 1O**). The averaged PV-positive (PV+) cell density in the whole brain was increased from P21 to P28 and gradually decreased with subsequent developmental stages (**Fig. 1P**, top panel). Similar trends were observed in many cerebral regions (**Fig. 1P**, middle panel), while the PV+ cell density decreased monotonically in all brain-stem regions (**Fig. 1P**, bottom panel). These changes could be attributed to PV+ cell loss rather than a decrease in PV expression in individual PV+ cells (**fig. S3, A to B**).

15

A detailed comparison of PV-neuron distribution in the P28 and P84 brains revealed subregion-specific changes in PV+ cell density (**Fig. 1, Q to R; fig. S3C**). Except for the visual (VIS) cortex, the PV+ cell density in P84 was lower than in P28 in almost all areas of isocortex (**Fig. 1R**). PV+ cell density in the somatomotor (MO) and anterior cingulate (ACA) cortex gradually decreased beginning at P28, whereas it increased or stabilized during the same period in the VIS cortex (**Fig. 1S**). The PV+ cell density in some cortical regions, such as the somatosensory (SS) cortex, changed little during development (**Fig. 1S**).

Cortical PV neurons are activated upon the prolonged wakefulness.

20

We investigated PV-neuron activity during SD to understand the physiological role of PV neurons in sleep homeostasis. After a 6-hour SD, mouse brains were collected for whole-brain immunostaining of PV and c-Fos proteins to investigate PV-neuron activity upon SD (**Fig. 2A**). A comparison of *ad libitum* sleep (Slp) and SD brains revealed that SD increased c-Fos-positive (c-Fos+) cell density in many brain regions (**Fig. 2B**). There was also an increase in c-Fos+ cell density among the PV+ cell population (i.e., c-Fos+PV+ cells), particularly in cortical regions (**Fig. 2C**). We also discovered that the SD increased the density of PV+ cell in the isocortex to some extent (**Fig. 2D**). The population of c-Fos+PV+ cells was higher in SD brains than in Slp brains in the isocortex (**Fig. 2, E to F; fig. S4, A to B**). Cortical c-Fos+PV+ cells were found to be increased in MK-801-treated brains (**Fig. 2, G to H; fig. S4, C to G**). These findings indicate that prolonged wakefulness increases cortical PV-neuron activity.

30

35

PV-enhancer-targeted (E11) neurons are necessary and sufficient for rebound sleep.

40

Next, we aimed to test the influence of PV-neuron activity on sleep architecture and homeostasis. Cortical PV neurons were targeted using E11, a PV-neuron selective enhancer derived from the *Pvalb* region (25), packaged in adeno-associated virus (AAV) vector (**fig. S5A**). Nuclear-localized mCherry signals under the E11 enhancer (E11-H2B-mCherry) were primarily detected in cerebral regions including the isocortex, and more than 80% of E11-labeled cells in the isocortex were PV+ cells (**fig. S5, B to E**). The cells targeted by this system were termed as E11 neurons after that.

We expressed a tetanus-toxin light-chain (TeLC) protein, which blocks synaptic transmission, in E11 neurons. TeLC expression in E11 neurons resulted in a negligible change in sleep duration but a significant increase in P_{ws} and P_{sw} (**fig. S5, F to H**). We also conducted chemogenetic

manipulations of E11-neuron activity (**Fig. 2I**). Mice expressing hM3Dq (E11-hM3Dq mice) had an increase in sleep duration after clozapine-*N*-oxide (CNO) administration (**Fig. 2J**; **fig. S5, I to J**). In the E11-hM3Dq-induced sleep state, increased P_{ws} and decreased P_{sw} were observed (**Fig. 2, K to L; fig. S5, K to N**), similar to the rebound phase after SD (**Fig. 1, E to G**). Chemogenetic suppression, on the other hand, resulted in an acute reduction in sleep duration with decreased P_{ws} and increased P_{sw} in mice expressing hM4Di (E11-hM4Di mice) (**Fig. 2, J to L; fig. S5, I to N**).

We hypothesized that E11-neuron activity is required for rebound sleep because acute enhancement of E11-neuron activity induced a rebound-sleep-like state (**Fig. 2, J to L; fig. S5, I to N**). To test this, we used chemogenetic inhibition of E11 neurons after SD (**Fig. 2M**). We used a lower CNO dosage that had little effect on the normal sleep-wake cycle (**fig. S6, A to G**). Even in this condition, E11-hM4Di mice had impaired rebound sleep after CNO administration (E11-hM4Di mice: SD+CNO), whereas normal rebound sleep was observed in the absence of CNO administration (E11-hM4Di mice: SD+Sal) (**Fig. 2, N to P**). Mice only expressing mCherry (E11-mCherry mice) exhibited normal rebound sleep with or without CNO administration (E11-mCherry mice: SD+Sal or SD+CNO) (**Fig. 2, N to P**). Rebound responses in P_{ws} and P_{sw} were also reduced in E11-hM4Di mice after CNO administration (**Fig. 2, Q to T**). These findings suggested that rebound sleep requires increased E11-neuron activity.

Inhibition of CaMKII activity in E11 neurons impairs sleep homeostasis.

We then concentrated on CaMKII as a key molecule since the phosphorylation states of CaMKII and its potential substrates in forebrain synapses change with sleep-wake states (26–28), and animals with CaMKII α/β genetic modification had abnormal sleep architecture (29, 30). Using single-cell RNA sequencing (scRNA-seq) data (31), we confirmed that all CaMKII isoforms (*Camk2a*, *Camk2b*, *Camk2g*, and *Camk2d*) were expressed in cortical PV neurons (**fig. S7, A to D**). Furthermore, using other scRNA-seq data (32), we found that *Camk2a* expression level and positive-cell rate in cortical PV neurons were higher in the adults compared to adolescents (**fig. S7, E to H**).

To see if CaMKII within PV neurons regulates sleep architecture and homeostasis based on its kinase activity, we inhibited the endogenous CaMKII activity in E11 neurons with CN19o, an optimized CaMKII inhibitory peptide (33) (**Fig. 3A**). Mice expressing CN19o under the E11 enhancer (E11-CN19o mice) showed no significant difference in sleep duration when compared to mice expressing CN19scr (E11-CN19scr mice) (**fig. S8A**), the CN19o scrambled sequence (**Fig. 3A**). However, the E11-CN19o mice had higher P_{ws} and P_{sw} than the E11-CN19scr mice (**fig. S8, B to C**), similar to E11-neuron chronic silencing (**fig. S5, F to H**).

We next performed a 6-hour SD on E11-CN19o and E11-CN19scr mice (**Fig. 3A**). Surprisingly, the E11-CN19o mice barely showed rebound sleep responses, whereas the E11-CN19scr mice clearly showed the responses following SD (**Fig. 3, B to F; fig. S8D**). After MK-801 administration, the E11-CN19o mice also showed lower rebound responses than the E11-CN19scr mice (**Fig. 3, G to K; fig. S8E**). These findings suggest that CaMKII kinase activity in E11 neurons is important for both basal sleep architecture and homeostatic sleep rebound.

We also recorded EEG and electromyogram (EMG) in E11-CN19o and E11-CN19scr mice. There was no significant difference in rapid eye movement (REM) sleep or non-REM (NREM) sleep duration between the E11-CN19o and E11-CN19scr mice (**Fig. 3, L to M**). The E11-CN19o mice, on the other hand, had higher transition probabilities between wake and NREM sleep states (i.e., increased W→N and N→W) and lower state stabilities (i.e., decreased W→W and N→N) (**Fig. 3N**). The level of delta (0.5–4.0 Hz) or slow oscillation (SO, 0.5–1.0 Hz) power during NREM

5

sleep is correlated with the level of sleep need (34, 35). The delta power in E11-CN19o mice decreased significantly during NREM sleep (Fig. 3, O to P; fig. S8, F to G). The SO power did not change significantly but did tend to decrease (Fig. 3O and fig. S8H). These findings show that decreased CaMKII activity in the E11 neurons reduces NREM sleep quality (i.e., its stability and delta power).

Elevation of CaMKII α activity in E11 neurons induces rebound-sleep-like state.

10

CaMKII α is activated by Ca^{2+} /calmodulin (CaM) binding and autophosphorylates threonine (T) 286 to maintain kinase activity even when Ca^{2+} /CaM is not present (36) (Fig. 4A). Thus, the T286 phosphomimetic mutant (T286D), in which the threonine (T) is replaced with aspartic acid (D), becomes constitutively kinase-active form (36). To see if CaMKII α activation in E11 neurons affects sleep phenotype, we expressed wild-type (WT) or T286D CaMKII α in E11 neurons. Mice expressing WT CaMKII α (E11-CaMKII α (WT) mice) showed no differences in all sleep parameters when compared to E11-EGFP mice (Fig. 4, B to D). In contrast, E11-CaMKII α (T286D) mice had significantly longer sleep duration, higher P_{ws} , and lower P_{sw} than E11-EGFP and E11-CaMKII α (WT) mice (Fig. 4, B to D). T286 non-phosphomimetic alanine (A) mutation (T286A) or kinase-dead mutation (K42R) adding to T286D (K42R:T286D) did not exhibit the changes of sleep parameters as observed in E11-CaMKII α (T286D) mice (fig. S9, A to C). The expression of constitutively active (T287D) CaMKII β in E11 neurons also resulted in a rebound-sleep-like state as well as CaMKII α activation (fig. S9, D to F).

20

CaMKII α (WT or T286D) was expressed in *Per1^{-/-}:Per2^{-/-}* (*Per* dKO) or *Cry1^{-/-}:Cry2^{-/-}* (*Cry* dKO) mice to see if the sleep-promoting effects of CaMKII α activation in E11 neurons were dependent on the circadian clock genes (Fig. 4E). Under constant dark (DD) conditions, these dKO lines exhibit arrhythmic-circadian behavior (22). Regardless of circadian time, E11-CaMKII α (T286D) mice in both dKO backgrounds kept under DD condition showed significantly longer sleep duration, higher P_{ws} , and lower P_{sw} (Fig. 4, F to H; fig. S9, G to L).

25

Given the rebound-sleep-like phenotype observed in E11-CaMKII α (T286D) mice (Fig. 4, B to D), it is reasonable to conclude that these mice have already acquired the saturated sleep need. To put this theory to the test, we performed a 6-hour SD on E11-CaMKII α (T286D) mice. The E11-CaMKII α (T286D) mice had rebound sleep characteristics even in basal sleep and only had marginal rebound sleep after the SD (fig. S9, M to Q). Similarly, after MK-801 administration, E11-CaMKII α (T286D) mice showed lower rebound responses (fig. S9, R to V).

30

Furthermore, we recorded EEG and EMG in E11-CaMKII α (WT) and E11-CaMKII α (T286D) mice. The increased sleep duration in the E11-CaMKII α (T286D) mice is due to an increase in NREM sleep (Fig. 4I), whereas REM sleep did not differ between groups (Fig. 4J). Consistent with this, E11-CaMKII α (T286D) mice had higher NREM sleep stability (i.e., increased N \rightarrow N) (Fig. 4K). The SO power was increased in E11-CaMKII α (T286D) mice, but the delta power changes were not significant (Fig. 4, L to M; fig. S10, A to C). These findings show that constitutive CaMKII α activation in E11 neurons increases both the quantity and quality of NREM sleep.

35

40 CaMKII activity in E11 neurons encodes sleep need.

CaMKII kinase activity in E11 neurons has similar effects on sleep homeostasis as E11-neuron activity manipulation. We thus hypothesized that CaMKII activation increases cortical PV-neuron activity, causing rebound sleep. To test this hypothesis, we performed double-immunostaining of PV and c-Fos proteins in brains of E11-CaMKII α (T286D) mice. The isocortex contained more

than three-quarters of the detected c-Fos+PV+ cells (**Fig. 5, A to B**). CaMKII α (T286D) expression in E11 neurons selectively enhanced c-Fos expression in cortical PV neurons (**Fig. 5, C to E**) but had little effect on the overall number of c-Fos+ or PV+ cells (**fig. S11, A to B**). These findings imply that intracellular CaMKII activation increases PV-neuron activity.

We next developed a system for measuring CaMKII α T286 autophosphorylation using liquid chromatography-tandem mass spectrometry (LC-MS/MS) with watermark-mutant (E285D) CaMKII α expression in E11 neurons (**Fig. 5F**), in which the glutamic acid (E) near T286 residue is replaced with aspartic acid (D). CaMKII α (E285D) is distinguishable from all endogenous CaMKII isoforms (**fig. S12A**), allowing us to selectively quantify the T286 autophosphorylation level of CaMKII α (E285D) expressed in the brain (**Fig. 5F**). We confirmed that CaMKII α (E285D) expression and kinase activity were nearly identical to WT CaMKII α (**fig. S12, B to C**). We also confirmed that no difference in any sleep parameters was observed between E11-CaMKII α (WT) and E11-CaMKII α (E285D) mice under basal and sleep-deprived conditions (**fig. S12, D to N**). We gave the E11-CaMKII α (E285D) mice a 6-hour SD and collected their isocortex immediately afterward. Using the LC-MS/MS analysis, we revealed that T286 phosphorylation (pT286) level derived from CaMKII α (E285D) increased in SD group compared to *ad libitum* sleep (Slp) group (**Fig. 5G**). These findings suggest that CaMKII α kinase activity in cortical PV neurons reflects the level of sleep need.

Discussion

We identified cortical PV neurons as a neural population responsible for homeostatic sleep rebound. Previous research has shown that subcortical and/or brain-stem regions regulate sleep homeostasis across the brain (2). However, as demonstrated by “local sleep,” brain-wide regulatory systems are unable to fully account for several aspects of sleep homeostasis (3). Recent research has revealed that cortical excitatory (pyramidal) neurons play a role in the regulation of sleep homeostasis (37). Our findings emphasize the importance of both cortical excitatory and inhibitory neurons in the regulation of sleep homeostasis. PV neurons can detect the synchronous firings of surrounding pyramidal neurons (38), and they can synchronize local circuit activity by inhibiting a number of surrounding pyramidal neurons (8, 39). Because synchronized cortical activity correlates with expected level of sleep need (40), cortical PV neurons may regulate the synchronicity of local cortical microcircuits and generate cortical slow waves in collaboration with other inhibitory neurons (41–43). The microcircuit is widespread: reciprocal connections between these two neural types are common across cortical areas/layers and species (44–47). The microcircuits may contribute to the local sleep homeostasis observed in mammalian cortex.

CaMKII α / β -dependent phosphorylation responds well to sleep-wake states and sleep need, according to phosphoproteomic studies (26–28). Previous research has shown that genetic deletion of CaMKII α / β or inhibition of CaMKII activity reduces daily sleep amount (29, 30). The kinase action in excitatory neurons promotes sleep, at least in part: expression of kinase-active CaMKII β mutant in excitatory neurons increases daily sleep amount (30). Our findings support the role of CaMKII in cortical PV neurons as a regulator of homeostatic sleep rebound. The molecular basis for the modulation is unknown, but it is possible that synaptic strength and/or intrinsic excitability in PV neurons are altered. Indeed, sleep-wake states influence electrophysiological activity and Ca²⁺ dynamics in cortical PV neurons (20, 21). CaMKII α kinase activity is required for the sleep-promoting effects (**fig. S9, A to C**), but the downstream targets (i.e., substrates) are not the core circadian clock factors (**Fig. 4, F to H; fig. S9, G to L**). The voltage-dependent K⁺ channels K_V3.1 and K_V3.3 may be important candidates because double knockout of these channels changes the electrophysiological properties of PV neurons and impairs rebound sleep (48).

We propose that CaMKII α is a key molecular factor in cortical PV neurons for encoding sleep need and inducing rebound sleep (Fig. 7H). The proposed mechanism may be responsible for local sleep homeostasis via the canonical negative feedback circuit in cortical inhibitory-excitatory neuron network (Fig. 7I). Such a regulatory motif for sleep homeostasis may be conserved across the animal kingdom: a distinct negative feedback circuit in flies is critical for sleep homeostasis regulation, with physiological properties modulated by sleep need (49). The design principle of the sleep homeostatic machinery may be shared by insects and mammals.

References and Notes

1. A. A. Borbély, S. Daan, A. Wirz-Justice, T. Deboer, The two-process model of sleep regulation: a reappraisal. *J. Sleep Res.* **25**, 131–143 (2016).
2. Y. Ma, G. Miracca, X. Yu, E. C. Harding, A. Miao, R. Yustos, A. L. Vyssotski, N. P. Franks, W. Wisden, Galanin Neurons Unite Sleep Homeostasis and α 2-Adrenergic Sedation. *Curr. Biol.* **29**, 3315–3322.e3 (2019).
3. J. M. Krueger, J. T. Nguyen, C. J. Dykstra-Aiello, P. Taishi, Local sleep. *Sleep Med. Rev.* **43**, 14–21 (2019).
4. R. Huber, M. F. Ghilardi, M. Massimini, G. Tononi, Local sleep and learning. *Nature* **430**, 78–81 (2004).
5. V. Vyazovskiy, A. A. Borbély, I. Tobler, Unilateral vibrissae stimulation during waking induces interhemispheric EEG asymmetry during subsequent sleep in the rat. *J. Sleep Res.* **9**, 367–371 (2000).
6. V. V. Vyazovskiy, U. Olcese, E. C. Hanlon, Y. Nir, C. Cirelli, G. Tononi, Local sleep in awake rats. *Nature* **472**, 443–447 (2011).
7. H. Hu, J. Gan, P. Jonas, Fast-spiking, parvalbumin+ GABAergic interneurons: From cellular design to microcircuit function. *Science* **345**, 1255263 (2014).
8. R. Tremblay, S. Lee, B. Rudy, GABAergic Interneurons in the Neocortex: From Cellular Properties to Circuits. *Neuron* **91**, 260–292 (2016).
9. T. Miyamae, K. Chen, D. A. Lewis, G. Gonzalez-Burgos, Distinct Physiological Maturation of Parvalbumin-Positive Neuron Subtypes in Mouse Prefrontal Cortex. *J. Neurosci.* **37**, 4883–4902 (2017).
10. B. W. Okaty, M. N. Miller, K. Sugino, C. M. Hempel, S. B. Nelson, Transcriptional and electrophysiological maturation of neocortical fast-spiking GABAergic interneurons. *J. Neurosci.* **29**, 7040–7052 (2009).
11. C. Itami, F. Kimura, S. Nakamura, Brain-derived neurotrophic factor regulates the maturation of layer 4 fast-spiking cells after the second postnatal week in the developing barrel cortex. *J. Neurosci.* **27**, 2241–2252 (2007).
12. E. M. Goldberg, H.-Y. Jeong, I. Kruglikov, R. Tremblay, R. M. Lazarenko, B. Rudy, Rapid developmental maturation of neocortical FS cell intrinsic excitability. *Cereb. Cortex* **21**, 666–682 (2011).
13. S. H. Bitzenhofer, J. A. Pöpplau, I. Hanganu-Opatz, Gamma activity accelerates during prefrontal development. *Elife* **9**, e56795 (2020).

14. A. Contractor, I. M. Ethell, C. Portera-Cailliau, Cortical interneurons in autism. *Nat. Neurosci.* **24**, 1648–1659 (2021).
- 5 15. E. Hashemi, J. Ariza, H. Rogers, S. C. Noctor, V. Martínez-Cerdeño, The Number of Parvalbumin-Expressing Interneurons Is Decreased in the Prefrontal Cortex in Autism. *Cereb. Cortex.* **27**, 1931–1943 (2017).
- 10 16. T. Wintler, H. Schoch, M. G. Frank, L. Peixoto, Sleep, brain development, and autism spectrum disorders: Insights from animal models. *J. Neurosci. Res.* **98**, 1137–1149 (2020).
17. D. Jouvet-Mounier, L. Astic, D. Lacote, Ontogenesis of the states of sleep in rat, cat, and guinea pig during the first postnatal month. *Dev. Psychobiol.* **2**, 216–239 (1970).
18. H. P. Roffwarg, J. N. Muzio, W. C. Dement, Ontogenetic Development of the Human Sleep-Dream Cycle. *Science.* **152**, 604–619 (1966).
19. A. B. Nelson, U. Faraguna, J. T. Zoltan, G. Tononi, C. Cirelli, Sleep patterns and homeostatic mechanisms in adolescent mice. *Brain Sci.* **3**, 318–343 (2013).
- 20 20. A. Brécier, M. Borel, N. Urbain, L. J. Gentet, *bioRxiv*, in press.
21. N. Niethard, S. Brodt, J. Born, Cell-Type-Specific Dynamics of Calcium Activity in Cortical Circuits over the Course of Slow-Wave Sleep and Rapid Eye Movement Sleep. *J. Neurosci.* **41**, 4212–4222 (2021).
22. G. A. Sunagawa, K. Sumiyama, M. Ukai-Tadenuma, D. Perrin, H. Fujishima, H. Ukai, O. Nishimura, S. Shi, R.-I. Ohno, R. Narumi, Y. Shimizu, D. Tone, K. L. Ode, S. Kuraku, H. R. Ueda, Mammalian Reverse Genetics without Crossing Reveals Nr3a as a Short-Sleeper Gene. *Cell Rep.* **14**, 662–677 (2016).
23. T. Mano, K. Murata, K. Kon, C. Shimizu, H. Ono, S. Shi, R. G. Yamada, K. Miyamichi, E. A. Susaki, K. Touhara, H. R. Ueda, CUBIC-Cloud provides an integrative computational framework toward community-driven whole-mouse-brain mapping. *Cell Reports Methods.* **1**, 100038 (2021).
24. E. A. Susaki, C. Shimizu, A. Kuno, K. Tainaka, X. Li, K. Nishi, K. Morishima, H. Ono, K. L. Ode, Y. Saeki, K. Miyamichi, K. Isa, C. Yokoyama, H. Kitaura, M. Ikemura, T. Ushiku, Y. Shimizu, T. Saito, T. C. Saido, M. Fukayama, H. Onoe, K. Touhara, T. Isa, A. Kakita, M. Shibayama, H. R. Ueda, Versatile whole-organ/body staining and imaging based on electrolyte-gel properties of biological tissues. *Nat. Commun.* **11**, 1982 (2020).
- 30 25. D. Vormstein-Schneider, J. D. Lin, K. A. Pelkey, R. Chittajallu, B. Guo, M. A. Arias-Garcia, K. Allaway, S. Sakopoulos, G. Schneider, O. Stevenson, J. Vergara, J. Sharma, Q. Zhang, T. P. Franken, J. Smith, L. A. Ibrahim, K. J. M Astro, E. Sabri, S. Huang, E. Favuzzi, T. Burbridge, Q. Xu, L. Guo, I. Vogel, V. Sanchez, G. A. Saldi, B. L. Gorissen, X. Yuan, K. A. Zaghloul, O. Devinsky, B. L. Sabatini, R. Batista-Brito, J. Reynolds, G. Feng, Z. Fu, C. J. McBain, G. Fishell, J. Dimidschstein, Viral manipulation of functionally distinct interneurons in mice, non-human primates and humans. *Nat. Neurosci.* **23**, 1629–1636 (2020).
- 35 26. F. Brüning, S. B. Noya, T. Bange, S. Koutsouli, J. D. Rudolph, S. K. Tyagarajan, J. Cox, M. Mann, S. A. Brown, M. S. Robles, Sleep-wake cycles drive daily dynamics of synaptic phosphorylation. *Science.* **366**, eaav3617 (2019).

27. G. H. Diering, R. S. Nirujogi, R. H. Roth, P. F. Worley, A. Pandey, R. L. Huganir, Homer1a drives homeostatic scaling-down of excitatory synapses during sleep. *Science*. **355**, 511–515 (2017).
- 5 28. Z. Wang, J. Ma, C. Miyoshi, Y. Li, M. Sato, Y. Ogawa, T. Lou, C. Ma, X. Gao, C. Lee, T. Fujiyama, X. Yang, S. Zhou, N. Hotta-Hirashima, D. Klewe-Nebenius, A. Ikkyu, M. Kakizaki, S. Kanno, L. Cao, S. Takahashi, J. Peng, Y. Yu, H. Funato, M. Yanagisawa, Q. Liu, Quantitative phosphoproteomic analysis of the molecular substrates of sleep need. *Nature*. **558**, 435–439 (2018).
- 10 29. F. Tatsuki, G. A. Sunagawa, S. Shi, E. A. Susaki, H. Yukinaga, D. Perrin, K. Sumiyama, M. Ukai-Tadenuma, H. Fujishima, R.-I. Ohno, D. Tone, K. L. Ode, K. Matsumoto, H. R. Ueda, Involvement of Ca(2+)-Dependent Hyperpolarization in Sleep Duration in Mammals. *Neuron*. **90**, 70–85 (2016).
- 15 30. D. Tone, K. L. Ode, Q. Zhang, H. Fujishima, R. G. Yamada, Y. Nagashima, K. Matsumoto, Z. Wen, S. Y. Yoshida, T. T. Mitani, Y. Arisato, R.-I. Ohno, M. Ukai-Tadenuma, J. Yoshida Garçon, M. Kaneko, S. Shi, H. Ukai, K. Miyamichi, T. Okada, K. Sumiyama, H. Kiyonari, H. R. Ueda, Distinct phosphorylation states of mammalian CaMKII β control the induction and maintenance of sleep. *PLoS Biol.* **20**, e3001813 (2022).
- 20 31. B. Tasic, Z. Yao, L. T. Graybuck, K. A. Smith, T. N. Nguyen, D. Bertagnolli, J. Goldy, E. Garren, M. N. Economo, S. Viswanathan, O. Penn, T. Bakken, V. Menon, J. Miller, O. Fong, K. E. Hirokawa, K. Lathia, C. Rimorin, M. Tieu, R. Larsen, T. Casper, E. Barkan, M. Kroll, S. Parry, N. V. Shapovalova, D. Hirschstein, J. Pendergraft, H. A. Sullivan, T. K. Kim, A. Szafer, N. Dee, P. Groblewski, I. Wickersham, A. Cetin, J. A. Harris, B. P. Levi, S. M. Sunkin, L. Madisen, T. L. Daigle, L. Looger, A. Bernard, J. Phillips, E. Lein, M. Hawrylycz, K. Svoboda, A. R. Jones, C. Koch, H. Zeng, Shared and distinct transcriptomic cell types across neocortical areas. *Nature*. **563**, 72–78 (2018).
- 25 32. A. Bhattacherjee, M. N. Djekidel, R. Chen, W. Chen, L. M. Tuesta, Y. Zhang, Cell type-specific transcriptional programs in mouse prefrontal cortex during adolescence and addiction. *Nat. Commun.* **10**, 4169 (2019).
33. S. J. Coultrap, K. U. Bayer, Improving a natural CaMKII inhibitor by random and rational design. *PLoS One*. **6**, e25245 (2011).
- 30 34. P. Franken, D. Chollet, M. Tafti, The homeostatic regulation of sleep need is under genetic control. *J. Neurosci.* **21**, 2610–2621 (2001).
- 35 35. C. Cirelli, R. Huber, A. Gopalakrishnan, T. L. Southard, G. Tononi, Locus ceruleus control of slow-wave homeostasis. *J. Neurosci.* **25**, 4503–4511 (2005).
36. K. U. Bayer, H. Schulman, CaM Kinase: Still Inspiring at 40. *Neuron*. **103**, 380–394 (2019).
37. L. B. Krone, T. Yamagata, C. Blanco-Duque, M. C. C. Guillaumin, M. C. Kahn, V. van der Vinne, L. E. McKillop, S. K. E. Tam, S. N. Peirson, C. J. Akerman, A. Hoerder-Suabedissen, Z. Molnár, V. V. Vyazovskiy, A role for the cortex in sleep-wake regulation. *Nat. Neurosci.* **24**, 1210–1215 (2021).
- 40 38. A. C. Kwan, Y. Dan, Dissection of cortical microcircuits by single-neuron stimulation in vivo. *Curr. Biol.* **22**, 1459–1467 (2012).
39. A. Kepecs, G. Fishell, Interneuron cell types are fit to function. *Nature*. **505**, 318–326 (2014).

40. V. V. Vyazovskiy, U. Olcese, Y. M. Lazimy, U. Faraguna, S. K. Esser, J. C. Williams, C. Cirelli, G. Tononi, Cortical firing and sleep homeostasis. *Neuron*. **63**, 865–878 (2009).
- 5 41. S. Zucca, G. D’Urso, V. Pasquale, D. Vecchia, G. Pica, S. Bovetti, C. Moretti, S. Varani, M. Molano-Mazón, M. Chiappalone, S. Panzeri, T. Fellin, An inhibitory gate for state transition in cortex. *eLife*. **6** (2017), doi:10.7554/eLife.26177.
- 10 42. S. Zucca, V. Pasquale, P. Lagomarsino de Leon Roig, S. Panzeri, T. Fellin, Thalamic Drive of Cortical Parvalbumin-Positive Interneurons during Down States in Anesthetized Mice. *Curr. Biol.* **29**, 1481-1490.e6 (2019).
- 15 43. M. Valero, T. J. Viney, R. Machold, S. Mederos, I. Zutshi, B. Schuman, Y. Senzai, B. Rudy, G. Buzsáki, Sleep down state-active ID2/Nkx2.1 interneurons in the neocortex. *Nat. Neurosci.* **24**, 401–411 (2021).
- 20 44. Y. Yoshimura, E. M. Callaway, Fine-scale specificity of cortical networks depends on inhibitory cell type and connectivity. *Nat. Neurosci.* **8**, 1552–1559 (2005).
- 15 45. A. M. Packer, R. Yuste, Dense, unspecific connectivity of neocortical parvalbumin-positive interneurons: a canonical microcircuit for inhibition? *J. Neurosci.* **31**, 13260–13271 (2011).
- 25 46. G. González-Burgos, L. S. Krimer, N. N. Urban, G. Barrionuevo, D. A. Lewis, Synaptic efficacy during repetitive activation of excitatory inputs in primate dorsolateral prefrontal cortex. *Cereb. Cortex*. **14**, 530–542 (2004).
47. G. González-Burgos, L. S. Krimer, N. V. Povysheva, G. Barrionuevo, D. A. Lewis, Functional properties of fast spiking interneurons and their synaptic connections with pyramidal cells in primate dorsolateral prefrontal cortex. *J. Neurophysiol.* **93**, 942–953 (2005).
- 25 48. F. Espinosa, M. A. Torres-Vega, G. A. Marks, R. H. Joho, Ablation of Kv3.1 and Kv3.3 potassium channels disrupts thalamocortical oscillations in vitro and in vivo. *J. Neurosci.* **28**, 5570–5581 (2008).
49. O. T. Shafer, A. C. Keene, The Regulation of Drosophila Sleep. *Curr. Biol.* **31**, R38–R49 (2021).

30 **Acknowledgments:** We would like to express our gratitude to S. Tomita and A. Shimokawa for their assistance with the SSS and EEG/EMG recordings, S. Sato as well as K. Shimizu for assisting with AAV production, Y. Saito for assisting with brain sample preparation, M. Kuroda (International Research Center for Neurointelligence, the University of Tokyo) for LSFM imaging technical assistance, and T. Jin (RIKEN BDR) for supporting with NMR analysis. We would like to thank Enago (www.enago.jp) for the English language review.

35 **Funding:** This work was supported by a Grant-in-Aid for JSPS Fellows (JSPS KAKENHI, 19J22074, to K.K.); a Grant-in-Aid for Scientific Research (C) (JSPS KAKENHI, 20K06576, to K.L.O.); a Grant-in-Aid for Early-Career Scientists (JSPS KAKENHI, 20K15766, to Y.S.); a Grant-in-Aid for Scientific Research (B) (JSPS KAKENHI, 22H02824, to E.A.S.); AMED-PRIME (JP20gm6210027, to E.A.S.); Grants-in-Aid from the Takeda Science Foundation and Nakatani foundation for advancement of measuring technologies in biomedical engineering (to E.A.S.); a Grant-in-Aid for Scientific Research (S) (JSPS KAKENHI, 18H05270, to H.R.U.); Human Frontier Science Program (HFSP) Research Grant Program (RGP0019/2018,

40

5 to H.R.U.); Exploratory Research for Advanced Technology (ERATO) (JST, JPMJER2001, to H.R.U.); Quantum Leap Flagship Program (Q-LEAP MEXT, JPMXS0120330644, to H.R.U.); Brain Mapping by Integrated Neurotechnologies for Disease Studies (Brain/MINDS) (AMED, JP21dm0207049, to H.R.U.); Innovative Drug Discovery and Development (AMED, JP19am0401011, to H.R.U.); and an intra-mural Grant-in-aid (RIKEN BDR, to H.R.U.).

10 **Author contributions:** K.K., K.L.O., and H.R.U. designed the study; S. Shi, and E.A.S. helped with the study design; K.K. performed the EEG/EMG recording, SD experiments, chemogenetic experiments, most sleep measurements using the SSS system and analyzed the data; H.F. and D.T. performed part of the SSS measurements; K.K., K.L.O., D.T., and S.Y. designed and constructed the plasmids; K.K. and C.S. produced AAVs; K.K., T.M., C.S., and S. Shiono performed the brain sample preparation, LSFM imaging, and data analysis; K.K., K.L.O., and R.R.T. performed biochemical experiments and analyzed the data; Y.S. synthesized CNO for preliminary chemogenetic experiments; R.G.Y. established the improved FASTER methods for EEG/EMG sleep staging; D.T., J.Y.G., M.K., K.S., and H.K. established the ES-cell-derived mice; K.K. prepared the figures and draft manuscript; K.K., K.L.O., and H.R.U. wrote the manuscript with input from all co-authors.

15

Competing interests: R.G.Y. and E.A.S. are employees of CUBICStars, Inc. H.R.U. is a founder and CTO of CUBICStars, Inc., which provides and maintains CUBIC-Cloud web service.

20 **Data and materials availability:** All data and materials used in this study are available from the corresponding author upon reasonable request.

Supplementary Materials

Materials and Methods

25 figs. S1 to S12

References and Notes

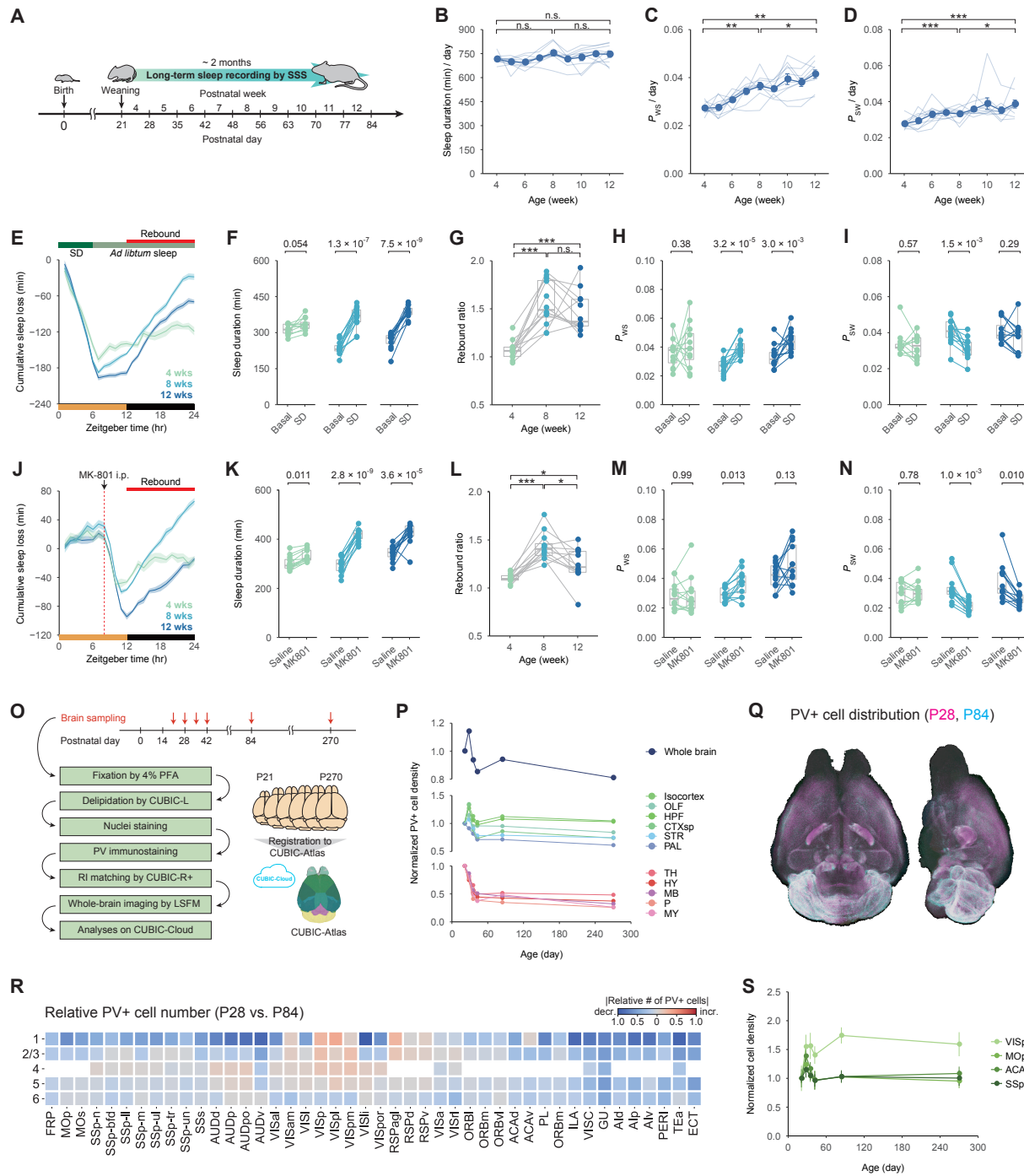


Fig. 1. Sleep architecture, sleep homeostasis, and PV-neuron distribution are altered along with development. (A) SSS-based long-term sleep phenotyping during post-weaning development (from P21 to P84). (B, C, and D) Daily sleep duration, P_{ws} , and P_{sw} in developing mice ($n = 10$). The blue points represent the average sleep parameters at each age. Each line (light blue) represents the sleep parameters of a single developing mouse. Welch's t -test with Bonferroni correction was used on mice aged 4, 8, and 12 weeks. (E) Cumulative sleep loss (SD – Basal) in mice aged 4, 8, and 12 weeks over 24 hours. (F, H, and I) Sleep duration, P_{ws} , and P_{sw} on Basal and SD during ZT12–24. At each age, the Welch's t -test was used to compare Basal and SD. (G)

Sleep rebound ratio (SD / Basal during ZT12–24). Individual mouse dots are connected by gray lines. Between the ages, the Welch's *t*-test with Bonferroni correction was used. (J) Cumulative sleep loss (MK-801 – Saline) in mice aged 4, 8, and 12 weeks over 24 hours. (K, M, and N) Sleep duration, *P_{ws}*, and *P_{sw}* on Saline and MK-801 during ZT12–24. At each age, the Welch's *t*-test was used to compare Saline and MK-801. (L) Sleep rebound ratio (MK-801 / Saline during ZT12–24). Individual mouse dots are connected by gray lines. Between the ages, Welch's *t*-test with Bonferroni correction was used. (O) Whole-brain analysis of PV+ cell distribution during post-weaning development. P21, P28, P35, P42, P84, and P270 mouse brains were collected ($n = 6$ for each age). Each set of whole-brain images was uploaded to the CUBIC-Cloud and registered to the CUBIC-Atlas brain. (P) The mean of PV+ cell density in the whole brain (top), cerebral regions (middle), and brain-stem regions (bottom) across post-weaning development ($n = 6$ for each age). Each point represents the mean value of each age normalized by P21. (Q) Representative whole-brain views of PV+ cell distribution from the dorsal and lateral sides at P28 (magenta) and P84 (cyan) ages. (R) A region-wise heat map of relative cell number depicting changes in PV+ cell number in the isocortex. P84 and P28 brains were compared, with red and blue colors indicating an increase and decrease, respectively. (S) Mean PV+ cell density across post-weaning development in selected cortical regions ($n = 6$ for each age). Each point represents the mean value of each age normalized by that of P21. Error bar: SEM, * $P < 0.05$, ** $P < 0.01$, *** $P < 0.001$, n.s. = non significance. Brain region acronyms follow the ontology defined by the Allen Brain Atlas.

5

10

15

20

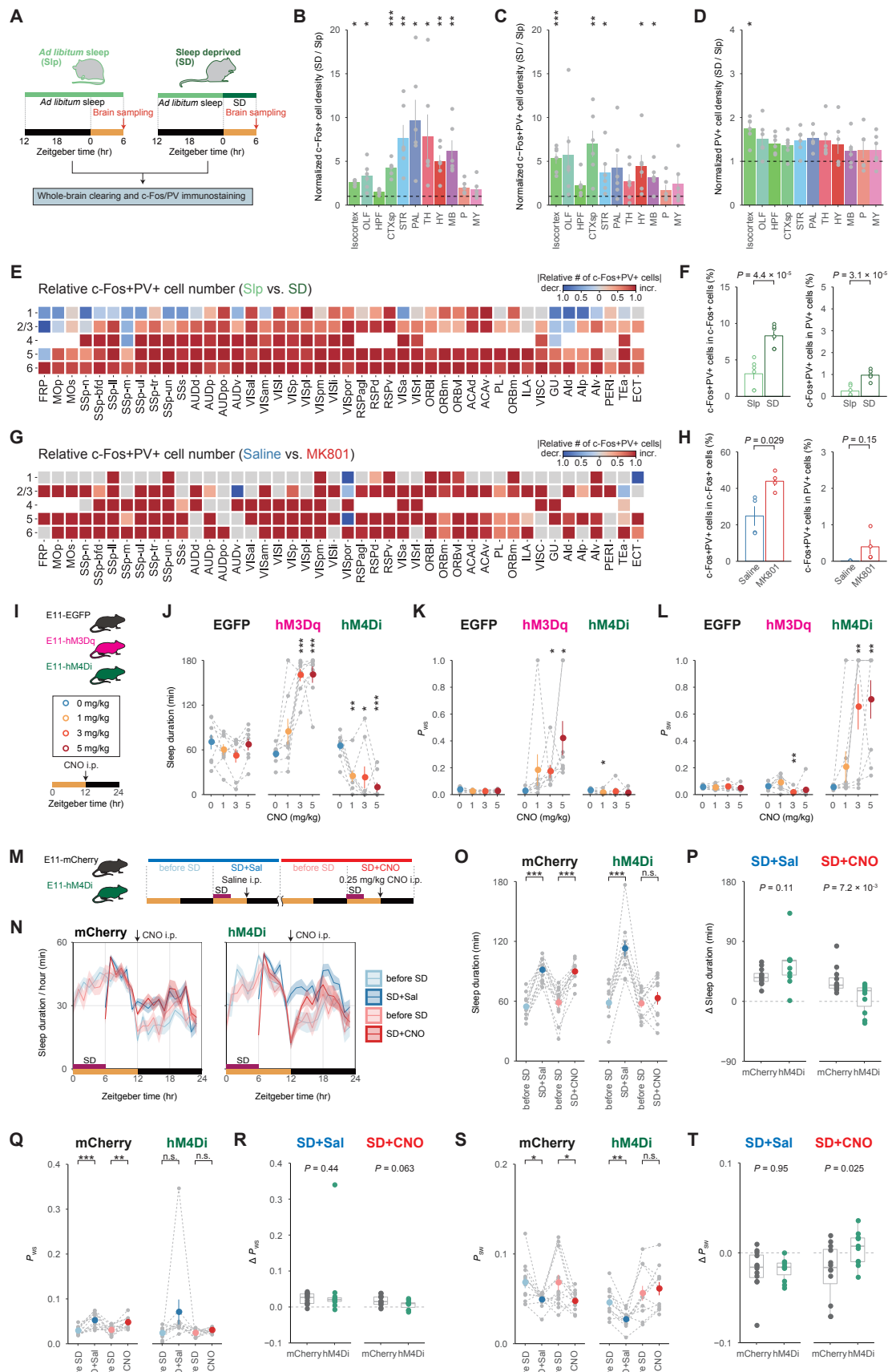


Fig. 2. PV-enhancer-targeted (E11) neurons are necessary and sufficient for rebound sleep.

(A) Experiment design for whole-brain analysis of c-Fos+ and/or PV+ cell distribution sleep-deprived condition. At ZT6, the brains of control (Slp) and sleep-deprived (SD) mice were collected ($n = 6$ for each group). Each set of whole-brain images was uploaded to the CUBIC-Cloud and registered to the CUBIC-Atlas brain. (B, C, and D) Normalized cell density (SD / Slp) of c-Fos+ cells, c-Fos+PV+ cells, and PV+ cells in major brain regions ($n = 6$ for each group). Each gray dot represents an individual SD brain normalized by the mean of Slp brains (mean = 1, black-dashed lines), and the colored bars represent the mean of SD brains in each brain region. The Welch's *t*-test was applied to the normalized value of Slp brains. (E and G) A region-wise heat map of relative cell number depicting changes in c-Fos+PV+ cell number in the isocortex. SD brains were compared to Slp brains, and MK-801-injected mouse (MK-801) brains were compared to control (Saline) brains, with red and blue colors indicating an increase and decrease, respectively. (F and H) Rate of double-positive (c-Fos+PV+) cells in c-Fos+ cells (left) or PV+ cells (right) in the isocortex under SD or MK-801 administration. The groups were compared using Welch's *t*-test. (I) Illustration of the CNO injection. Each mouse received i.p. injection in turn: 0 (blue), 1 (gold), 3 (red), or 5 (dark red) mg/kg CNO injection at ZT12, with at least 2 days between injections. (J, K, and L) Sleep duration, P_{ws} , and P_{sw} on the days with CNO injection during ZT12–15 ($n = 8$ for each group). Each gray dot represents an individual mouse, while colored dots represent the mean in each condition. Individual's mouse dots are connected by gray-dashed lines. Within the groups, Welch's *t*-test were run against the 0 mg/kg CNO condition. (M) Schematic diagram of CNO injection after sleep deprivation (SD). Every mouse received i.p. injection after a 6-hour SD during ZT0–6. At ZT12, 0 (blue, SD+Sal) or 0.25 (red, SD+CNO) mg/kg CNO injection was given. One day before the scheduled day with SD and i.p. injections are labeled "before SD." (N) Sleep duration over 24 hours in E11-mCherry ($n = 12$) and E11-hM4Di ($n = 11$) mice on SD+Sal (blue), SD+CNO (red), and "before SD" (light blue and salmon) days. (O, Q, and S) Sleep duration, P_{ws} , and P_{sw} on the days shown in the panel (N) during ZT12–15. Each gray dot represents an individual mouse, while the colored dots represent the mean in each condition. Individual mouse dots are connected by gray-dashed lines. Welch's *t*-test was used to compare the day with SD to the day "before SD." (P, R, and T) The differences (Δ) in sleep duration, P_{ws} , and P_{sw} between SD day during and the "before SD" day during ZT12–15. Welch's *t*-test was used to compare the groups in the SD+Sal or SD+CNO conditions. Error bar: SEM, $*P < 0.05$, $**P < 0.01$, $***P < 0.001$, n.s. = non significance. Brain region acronyms follow the ontology defined by the Allen Brain Atlas.

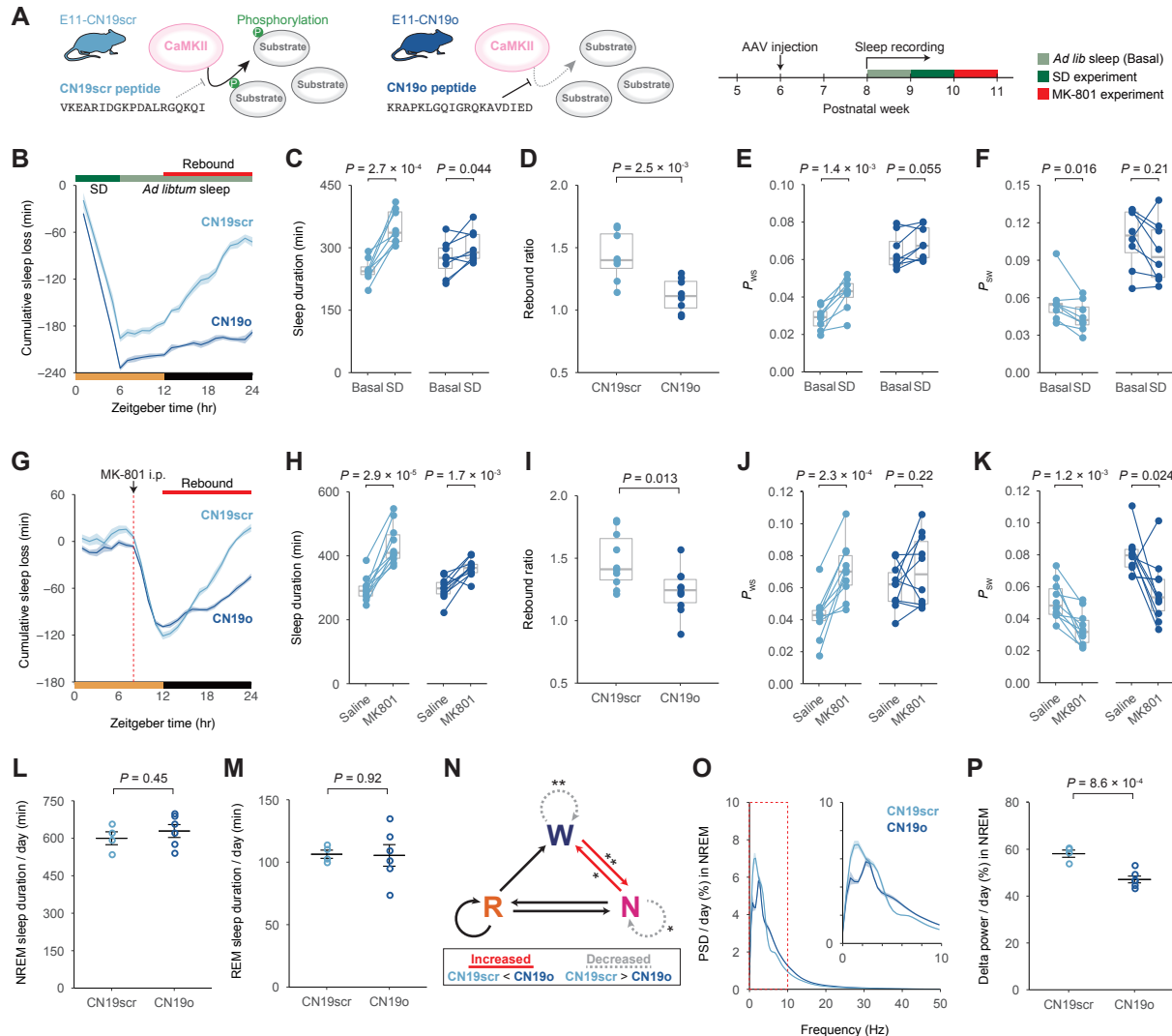


Fig. 3. Inhibition of CaMKII activity in E11 neurons inhibits rebound sleep. (A) Diagram of CaMKII inhibition by CN19o peptide (left) and experimental schedule (right). (B) Cumulative sleep loss (SD – Basal) in E11-CN19o (navy) and E11-CN19scr (light blue) mice over 24 hours ($n = 8$ per group). Mice were allowed to behave freely for three days prior to SD, and the averaged value of sleep parameters is shown as “Basal.” (C, E, and F) Sleep duration, P_{ws} , and P_{sw} on Basal and SD during ZT12–24. Student’s paired t -test was performed between Basal and SD within the groups. (D) Sleep rebound ratio (SD / Basal during ZT12–24). The groups were compared using Welch’s t -test. (G) Cumulative sleep loss (MK-801 – Saline) in E11-CN19o (navy) and E11-CN19scr (light blue) mice over 24 hours ($n = 10$ for each group). During the three days preceding the injections, the mice behaved normally. Each mouse received i.p. injection in turn: saline or 2 mg/kg MK-801 injection at ZT8, allowing at least 2 days between injections. (H, J, and K) Sleep duration, P_{ws} , and P_{sw} on days with saline or MK-801 injection during ZT12–24. The Student’s paired t -test was used to compare the saline and MK-801 injections within the groups. (I) Sleep rebound ratio (MK-801 / Saline during ZT12–24). The groups were compared using Welch’s t -test. (L and M) Daily NREM sleep duration and REM sleep duration in E11-CN19scr ($n = 4$, light blue) and E11-CN19o ($n = 6$, navy) mice. The groups were compared using Welch’s t -test. (N) Schematic of the sleep circuit showing Wake (W), Non-REM (N), and REM (R) states. Increased CN19scr < CN19o and Decreased CN19scr > CN19o are indicated. (O) Power Spectral Density (PSD) / day (%) in NREM for E11-CN19scr and E11-CN19o mice. The CN19o group shows a significant increase in Delta power (0–4 Hz) compared to CN19scr. (P) Delta power / day (%) in NREM for E11-CN19scr and E11-CN19o mice. The CN19o group shows a significant increase in Delta power compared to CN19scr.

5

The differences in transition probabilities between wake, NREM, and REM sleep states in E11-CN19o mice versus E11-CN19scr mice. The solid red and dotted gray lines represent a significant increase and decrease, respectively. (O) Power spectral density (PSD) of the EEG during NREM sleep. The extracted diagram in the 0–10 Hz range is also shown in the top-right corner of the panel. (P) Normalized delta power (0.5–4 Hz) during NREM sleep. The groups were compared using Welch's *t*-test. Error bar: SEM, **P* < 0.05, ***P* < 0.01, ****P* < 0.001, n.s. = non significance.

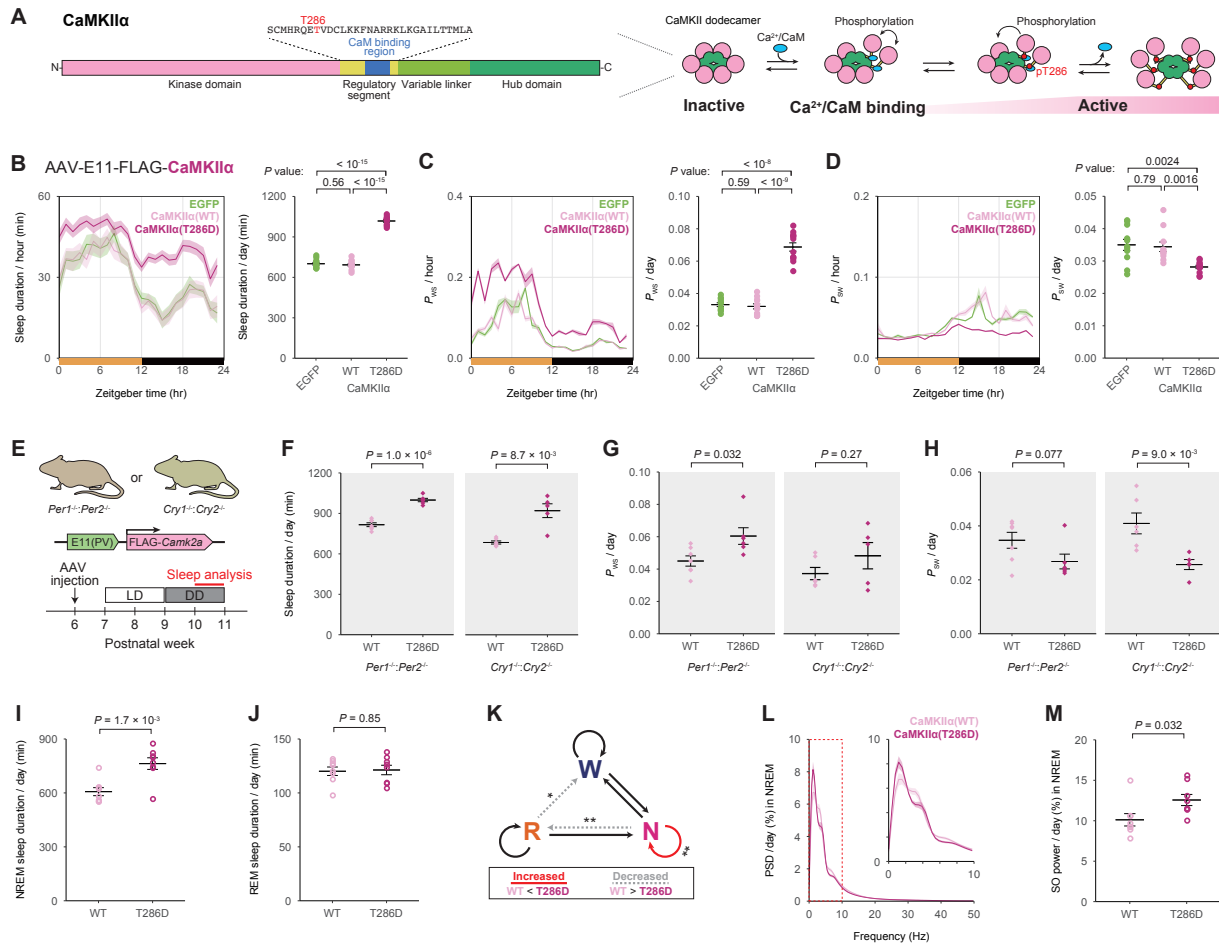


Fig. 4. Elevation of CaMKIIα activity in E11 neurons induces rebound-sleep-like state. (A) Illustration of CaMKIIα protein sequences (left) and endogenous CaMKIIα activation mechanism (right). The phosphorylation of T286 residue in the regulatory segment is critical for CaMKIIα activity regulation. **(B, C, and D)** Daily sleep duration, P_{ws} , and P_{sw} in E11-EGFP ($n = 11$, light green), E11-CaMKIIα (WT) ($n = 11$, pink), and E11-CaMKIIα (T286D) ($n = 12$, violet-red) mice. The groups were compared using Welch's t -test. It should be noted that the significance level of P -values is corrected using the Bonferroni correction. **(E)** Diagram of CaMKII expression and experimental schedule in *Per* or *Cry* dKO mice under constant dark conditions. **(F, G, and H)** Daily sleep duration, P_{ws} , and P_{sw} in the *Per* (left) or *Cry* (right) dKO mice expressing E11-CaMKIIα (WT) ($n = 7$, pink) or E11-CaMKIIα (T286D) ($n = 6$, violet-red). The groups were compared using Welch's t -test. **(I and J)** Daily NREM sleep duration and REM sleep duration in E11-CaMKIIα (WT) ($n = 8$, pink) and E11-CaMKIIα (T286D) ($n = 8$, violet-red) mice. The groups were compared using Welch's t -test. **(K)** The difference in transition probabilities between wake, NREM, and REM sleep states in E11-CaMKIIα (T286D) mice versus E11-CaMKIIα (WT) mice. The solid red and dotted gray lines represent a significant increase and decrease, respectively. **(L)** Power spectral density (PSD) of the EEG during NREM sleep. The extracted diagram in the 0–10 Hz range is also shown in the top-right corner of the panel. **(M)** Normalized slow-oscillation power (SO, 0.5–1Hz) during NREM sleep. The groups were compared using Welch's t -test. Error bar: SEM, * $P < 0.05$, ** $P < 0.01$, *** $P < 0.001$, n.s. = non significance.

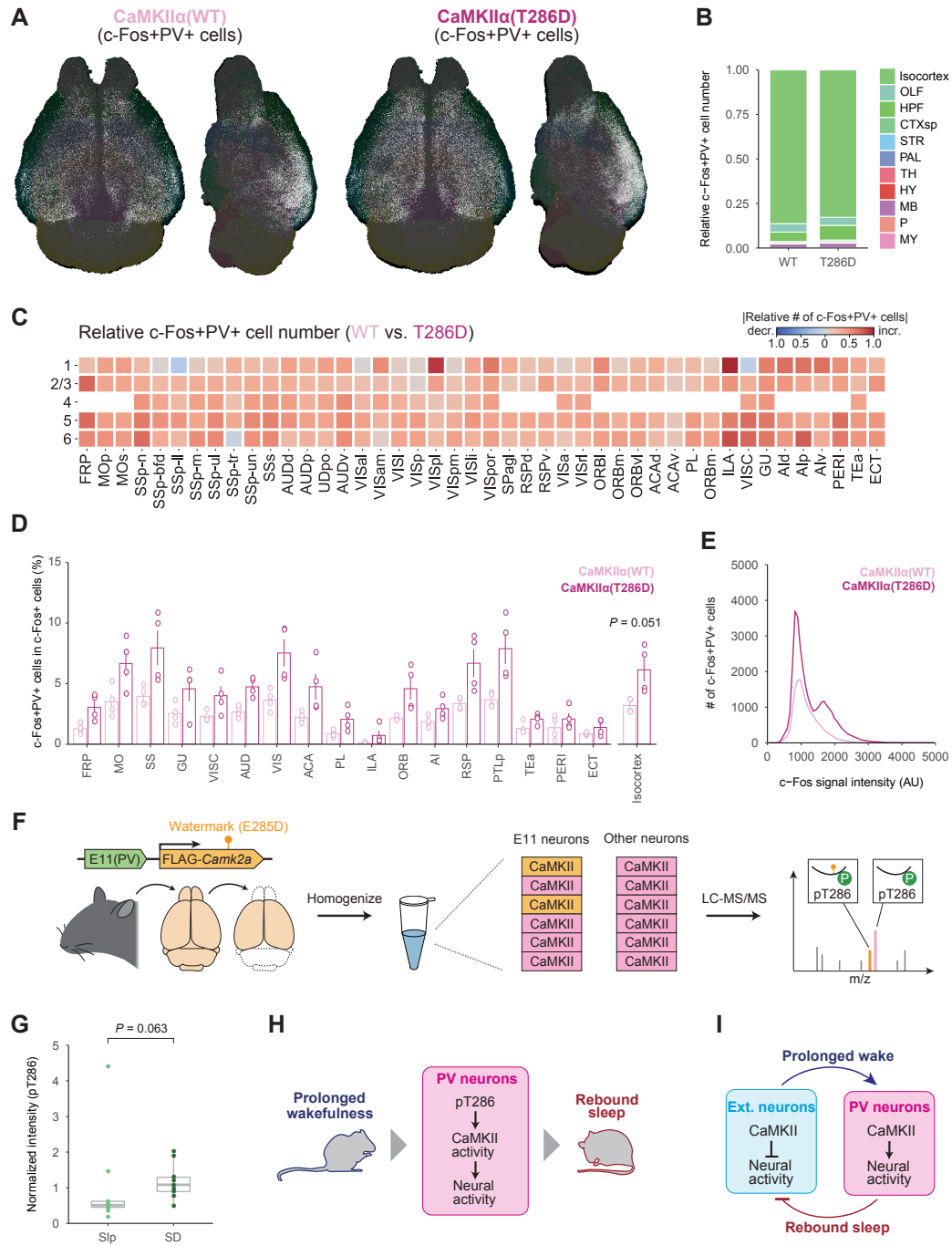


Fig. 5. CaMKII activity in E11 neurons encodes sleep need. (A) Representative whole-brain views of dorsal and lateral double-positive (c-Fos+PV+) cell distribution (white). The brains of E11-CaMKII α (WT) (left) and E11-CaMKII α (T286D) (right) mice were collected. (B) Stacked percentage bar plots of c-Fos+PV+ cells in the E11-CaMKII α (WT) and E11-CaMKII α (T286D) brains ($n = 4$ for each group). The plot depicts the demographics of c-Fos+PV+ cells in major brain regions. (C) A region-wise heat map of relative cell number showing changes in c-Fos+PV+ cell number in the isocortex. The E11-CaMKII α (T286D) brains were compared to the E11-CaMKII α (WT) brains, with red indicating an increase and blue indicating a decrease. (D) The rate of double-

positive (c-Fos+PV+) cells in c-Fos+ cells in each cortical region (left) or entire isocortex (right). The groups were compared using Welch's *t*-test. (E) The cortical distribution of c-Fos signal intensity per c-Fos+PV+ cell in each group. (F) Experimental design for quantitative analysis of CaMKII α T286 phosphorylation in E11 neurons. E11-CaMKII α (T285D) mice were dissected, and homogenates were used for LC-MS/MS analysis. (G) Signal intensities of peptides derived from CaMKII α (T285D) with phosphorylated T286 residues ($n = 9$ for each group). The intensities were normalized to the total CaMKII α level, which was calculated using all quantifiable non-phosphorylated peptides derived from WT CaMKII α . A two-sample Wilcoxon *t*-test was used to compare the groups. (H) CaMKII-dependent activity regulation of cortical PV neurons for homeostasis regulation. (I) Cortical feedback circuit model for sleep homeostasis regulation. Error bar: SEM. Brain region acronyms follow the ontology defined by the Allen Brain Atlas.